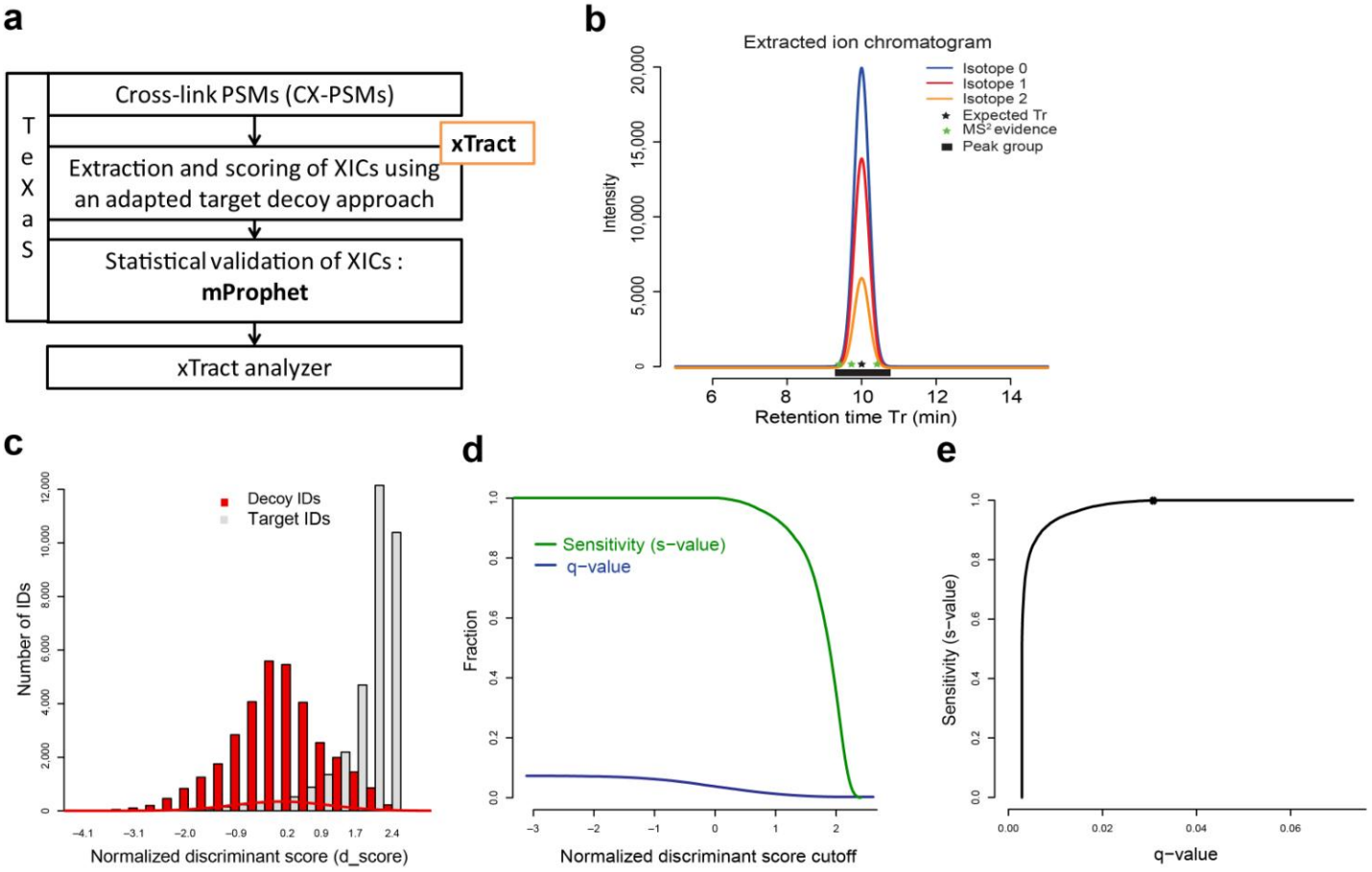

Supplementary Figure 1

Targeted extraction and statistical validation of ion chromatograms (TeXaS).

(**a**) Workflow of the TeXaS algorithms developed to quantify and validate ion chromatograms from cross-linked peptides from data dependent analysis MS experiments. (**b**) Model of an extracted ion chromatogram of a cross-linked peptide ion showing the extracted ion chromatograms of the individual isotopes. (**c**) Statistics on all extracted ion chromatogram peak groups generated by mProphet. (**d**) Sensitivity and q-value vs. the normalized discriminant score. (**e**) Sensitivity and q-value. The data point at which the sensitivity reaches its maximum is indicated by the dot. This corresponds to the maximal q-value that is used to further process the peak groups.

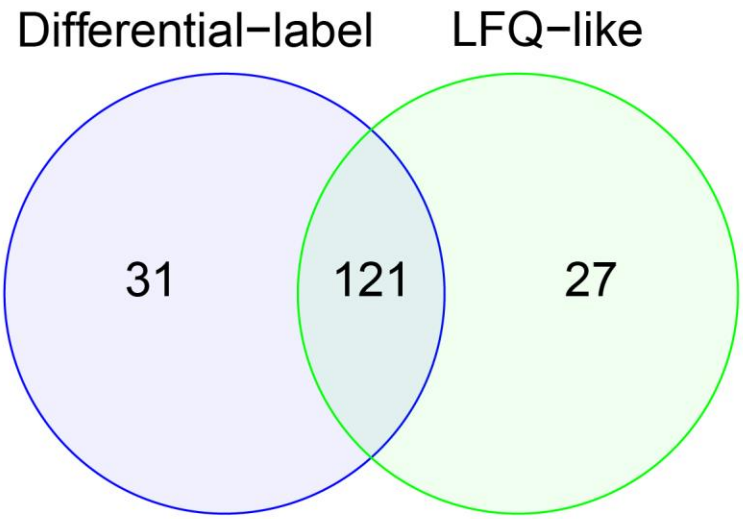

Supplementary Figure 2

Overlap of cross-linked peptides between different workflows of the dilution series dataset of model proteins.

In total 179 unique cross-linked peptides were identified across both experiments, 121 cross-linked peptides were in common between the differential isotopic label workflow and the LFQ-like workflow, 148 cross-links were identified by the LFQ-like workflow and 152 by the differential isotopic label workflow. The cross-links were validated using xProphet with an FDR cutoff of 5%.

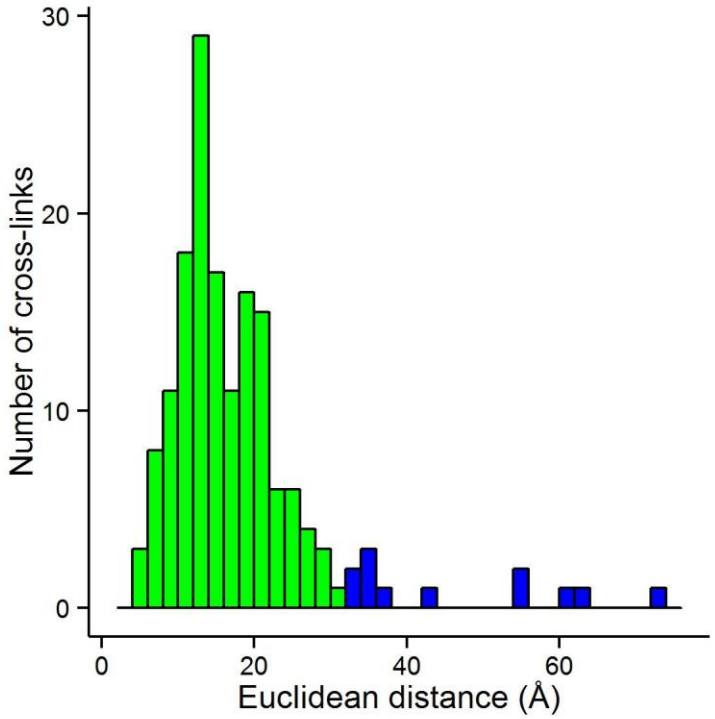

Supplementary Figure 3

Histogram of measured C_α distances of cross-links from the dilution series dataset.

Validation of the cross-links from the dilution series dataset of model proteins on the available protein structures or homology models of BSA, transferrin and conalbumin (see also Online methods). Out of 270 cross-links that were mapped onto the structures from the different workflows 12 cross-links exceeded the distance threshold of 32 Å (blue). This corresponds to 4.4 % of all validated cross-links and is in good agreement with the selected FDR cutoff of 5%.

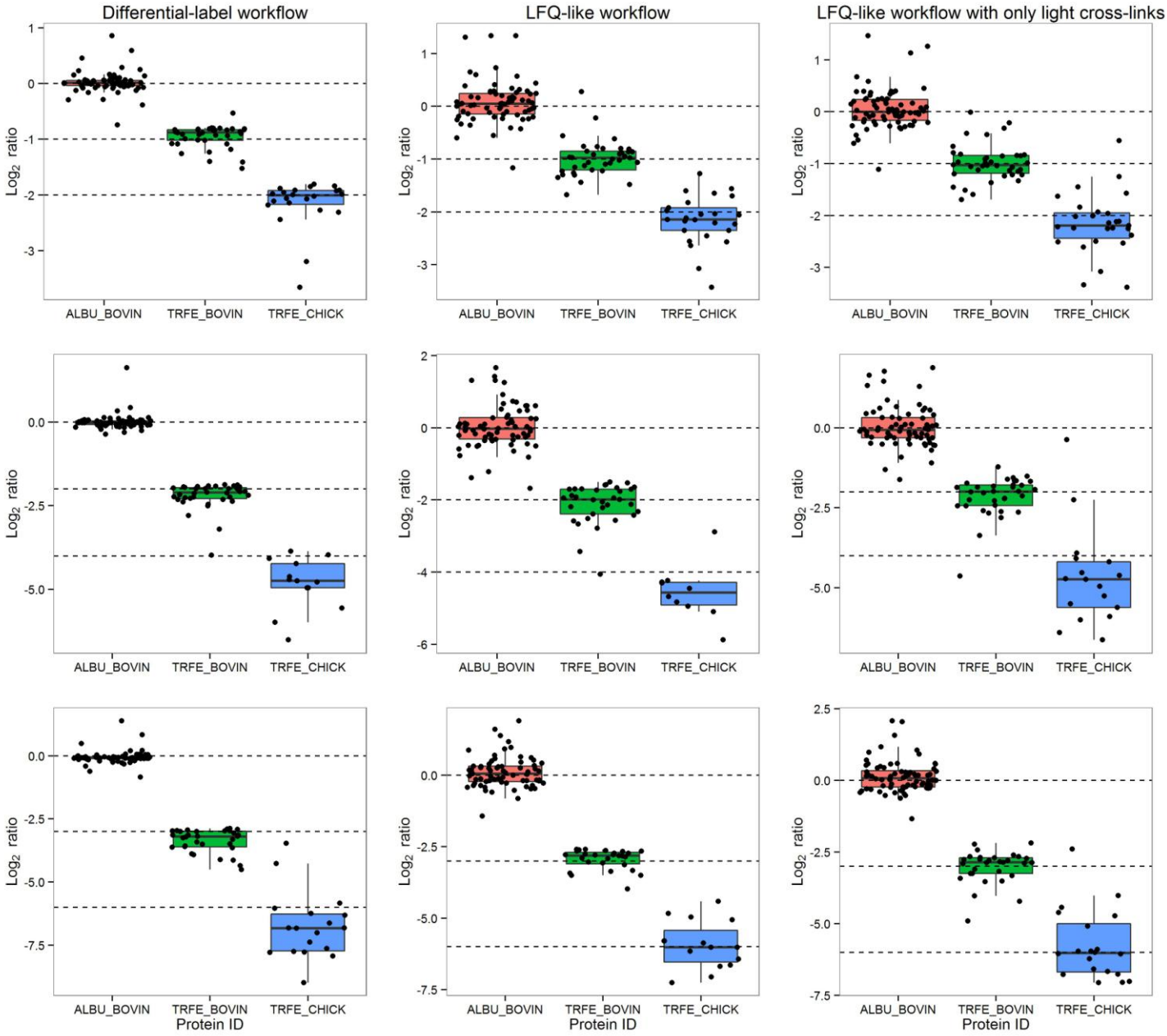

Supplementary Figure 4

Quantification results from the dilution series benchmarking dataset.

Shown are box plots and individual data points of the different cross-links from the different proteins that were mixed in defined ratios. The figure is divided into three columns (corresponding to the different workflows and the LFQ-like workflow when using only light cross-links) and three rows corresponding to the different dilutions (Samples 2-4) as outlined in **Supplementary Table 1**. The horizontal dotted lines indicate the expected values for the individual proteins. Bars within the box plot indicate the median values. Upper and lower hinges correspond to the first and third quartiles, whiskers correspond to +/- 1.5x the inter-quartile range.

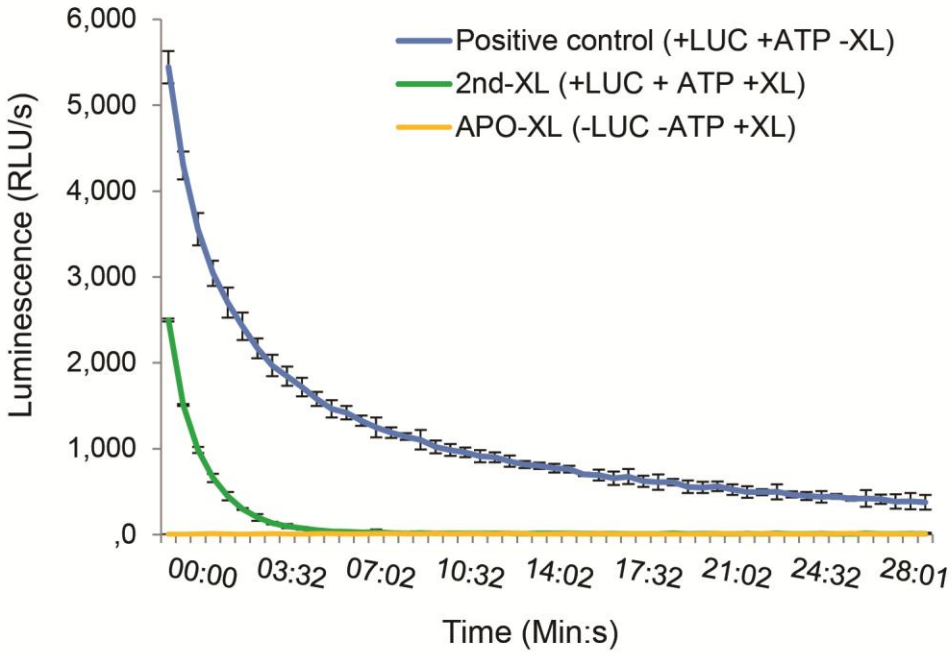

Supplementary Figure 5

Luminescence measurements during the cross-linking reaction of luciferase.

Shown is the decrease in luminescence during the cross-linking reaction (green line, +XL) compared to the positive control (blue line, -XL), both in presence of luciferin (LUC) and ATP. The yellow line shows the negative control (no luciferin and ATP). Data presented as mean ± s.d.

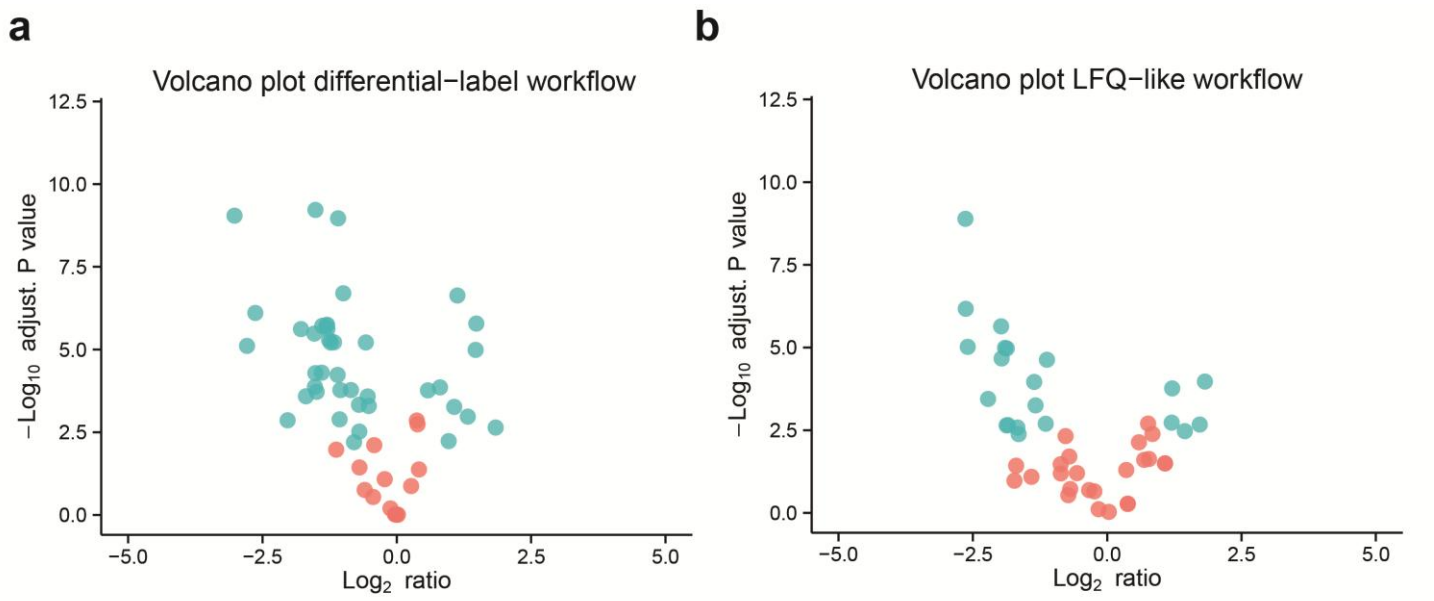

Supplementary Figure 6

Quantitative analysis of cross-links from the luciferase dataset.

(**a**) Volcano plot from the differential isotopic label workflow. (**b**) Volcano plot from the LFQ-like workflow. In the volcano plots the $\log_2$ ratios are plotted against the adjusted negative $\log_{10}$ *P* values. Indicated by color is if the observed changes are significant (blue) or not (red) (adjusted *P* value < 0.01 and absolute $\log_2$ fold change >1). The $\log_2$ ratios are shown with the apo experiment used as reference.

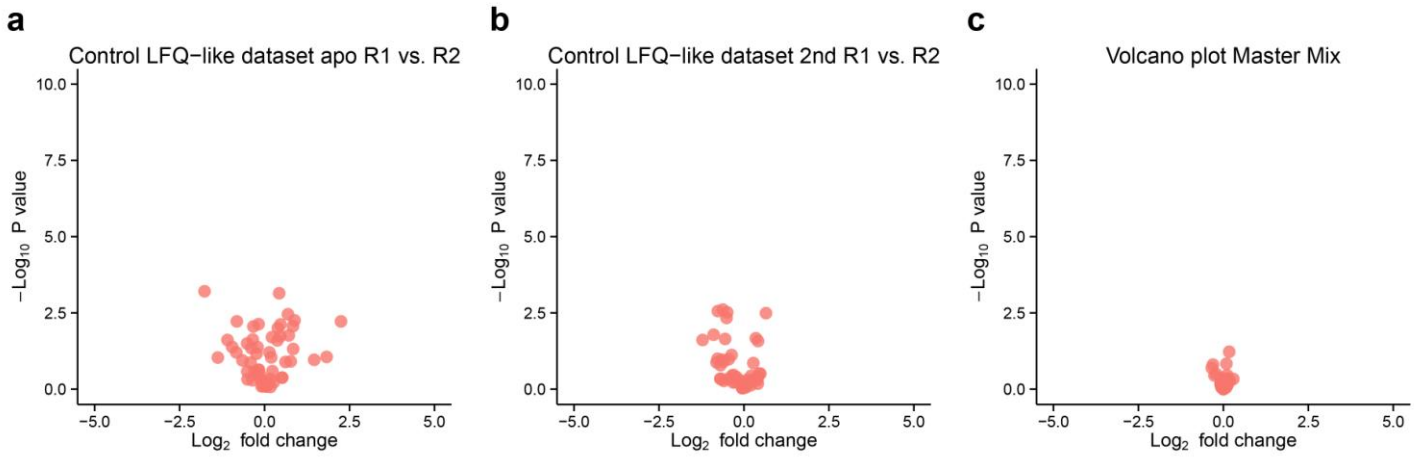

Supplementary Figure 7

Luciferase control experiments.

Shown in figure (**a**) and (**b**) are the $\log_2$ fold changes and negative $\log_{10}$ P values of the cross-links for the LFQ-like experiment by comparing different biochemical replicates against each other. Figure (**c**) shows the $\log_2$ fold changes of the cross-links for the Master Mix experiment, where light label is compared to the heavy labeled sample. Indicated by color is if the observed changes are significant (blue) or not (red) (adjusted *P* value < 0.01 and absolute $\log_2$ fold change >1).

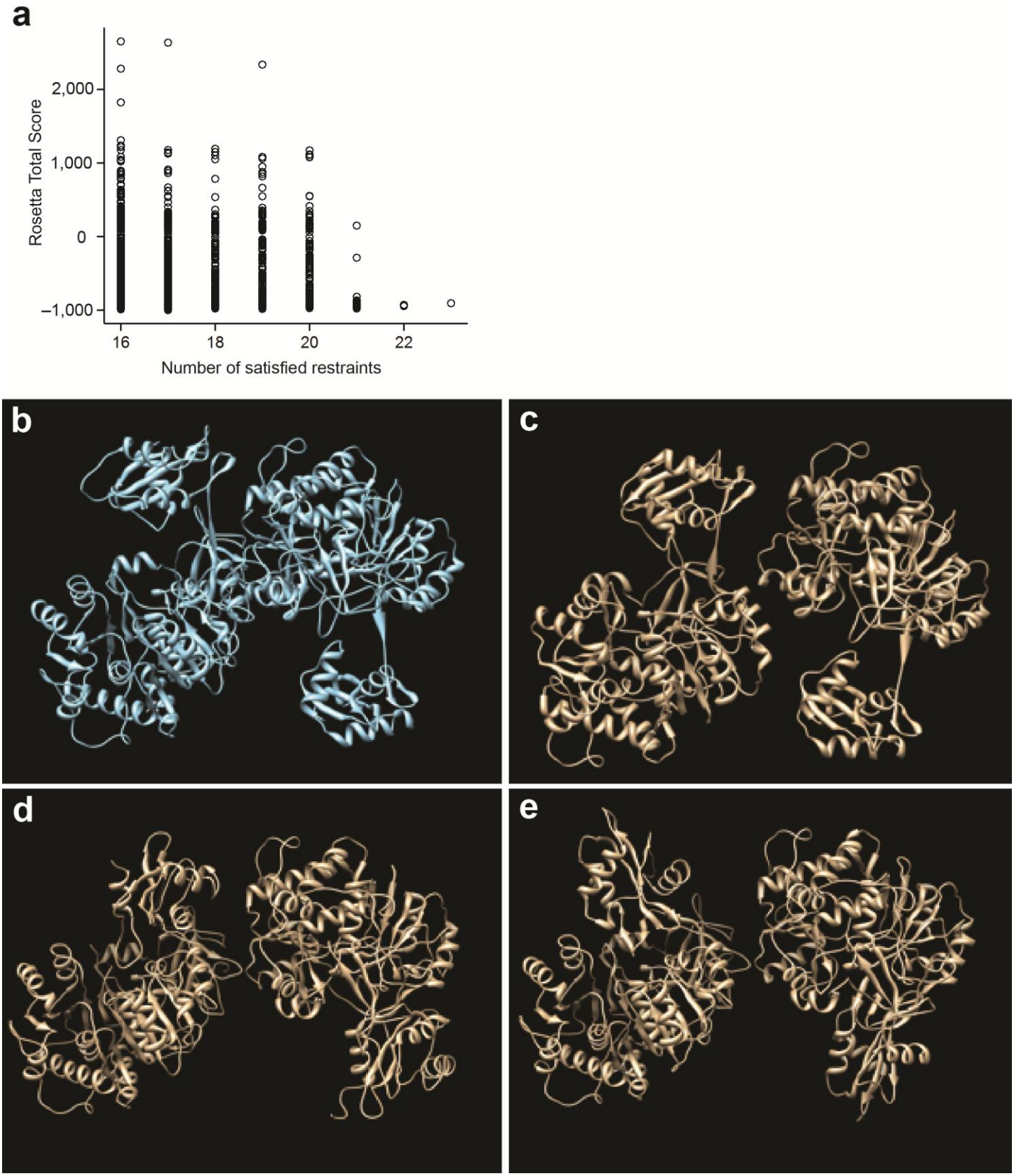
a
Rosetta Total Score
2,000
1,000
0
–1,000
16
18
20
22
Number of satisfied restraints
b
c
d
e

Supplementary Figure 8

Docking analysis and structural models of luciferase.
(**a**) Docking analysis, shown are the Rosetta energy score and the number of satisfied restraints for the models generated by the docking analysis, (**b**) Manual solution of the luciferase dimer, (**c**) Best (highest number of satisfied restraints) docking model of the luciferase dimer, (**d**) Dimer model of luciferase in the alternative conformation where luciferase is bound to the nucleotide analog DLSA (based on PDB ID 4G36) (**e**) Dimer model of luciferase in the alternative conformation where luciferase was stalled in a secondary conformation using a cysteine cross-linking approach (based on PDB ID 4G37).

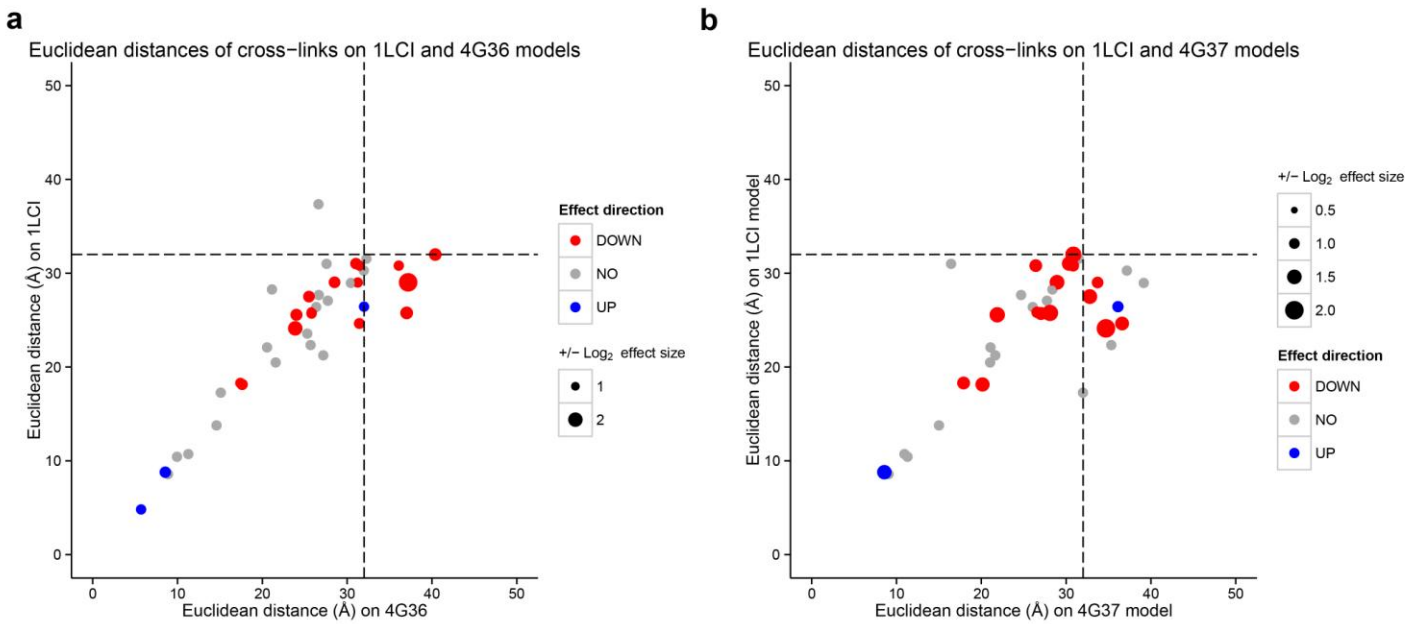

Supplementary Figure 9

Quantitative changes measured by qCX-MS on luciferase.

(**a**) Quantitative differences and Euclidean distances (Å) comparing apo (PDB ID 1LCI) to the alternative conformation of luciferase (PDB ID 4G36). (**b**) shows the comparison of apo (PDB ID 1LCI) to the secondary conformation described by the PDB ID 4G37. 2 FP cross-links exceeding the distance threshold of the cross-linker on both models are not shown. Colors red and blue indicate significantly changed uxIDs (adjusted *P* value <0.01 and absolute $\log_2$ fold change >1).

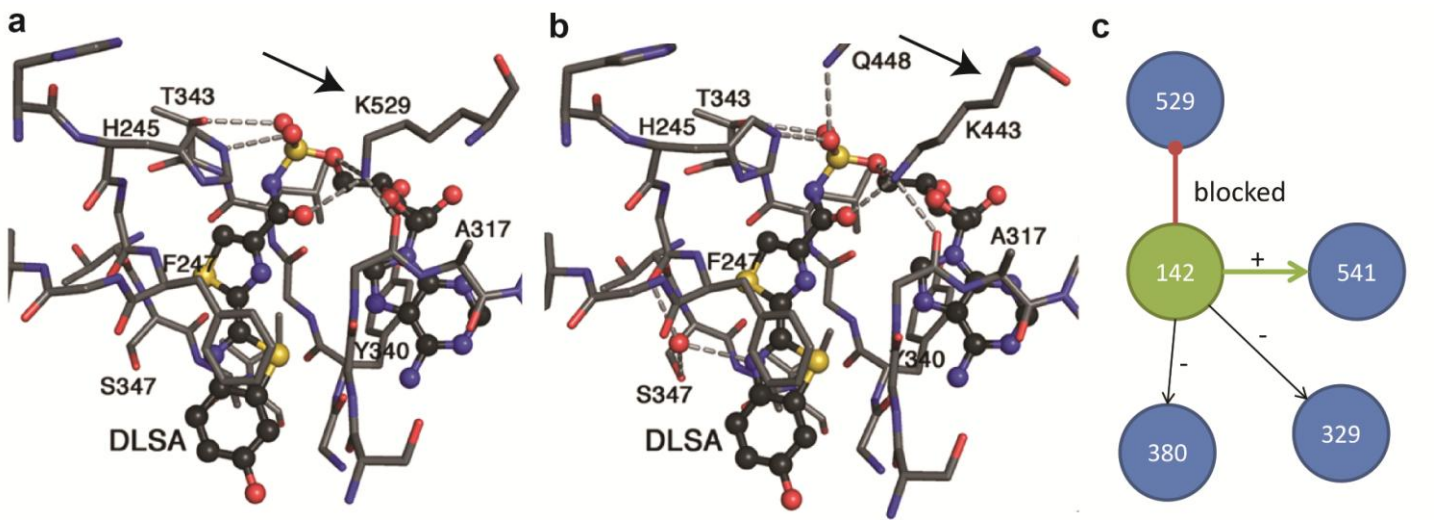

Supplementary Figure 10

Proposed network effect model explaining the quantitative behavior of the indicated cross-links.

(**a**) and (**b**): Stereo view of the active site of luciferase with bound DLSA in two different conformations (PDB ID 4G36 and 4G37). The residues Lys529 and Lys443 which contact the substrate are indicated by arrows. Adapted with permission from Sundlov, J. A., Fontaine, D. M., Southworth, T. L., Branchini, B. R. & Gulick, A. M. (2012). Biochemistry 51, 6493-6495. Copyright 2012 American Chemical Society. (**c**) Proposed model suggesting that inhibition of the formation of the cross-link between Lys142 and Lys529, which is blocked by the substrate binding, leads to the dominant cross-link 142-541 which shows a twofold increase in the second conformation. At the same time the cross-links 142-380 and 142-329 show a decreased abundance in the second confirmation presumably due to the dominant cross-link 142-541 and structural rearrangements.

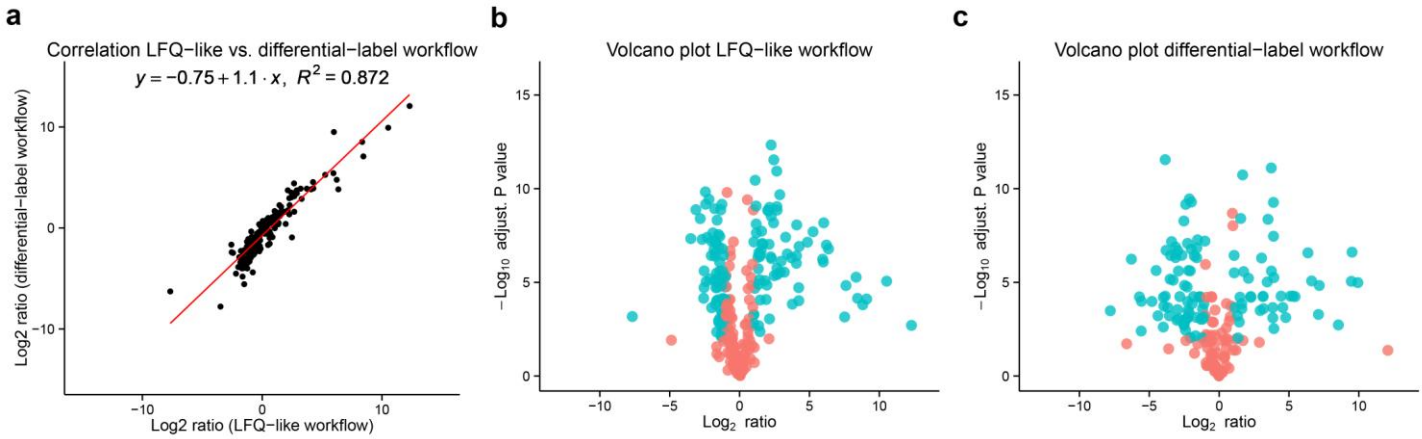

Supplementary Figure 11

Correlation and volcano plots of the TRiC apo and ATP-AlFx datasets using different quantitative cross-linking workflows.

(**a**) Correlation of common data points between the LFQ-like workflow and the differential isotopic label workflow. (**b**) Volcano plot of the LFQ-like workflow. (**c**) Volcano plot of the differential isotopic label workflow. In the volcano plots the $\log_2$ ratios are plotted against the adjusted negative $\log_{10}$ *P* values. Indicated by color is if the observed changes are significant (blue) or not (red) (adjusted *P* value < 0.01 and absolute $\log_2$ fold change >1). The $\log_2$ ratios are shown with the apo experiment used as reference.

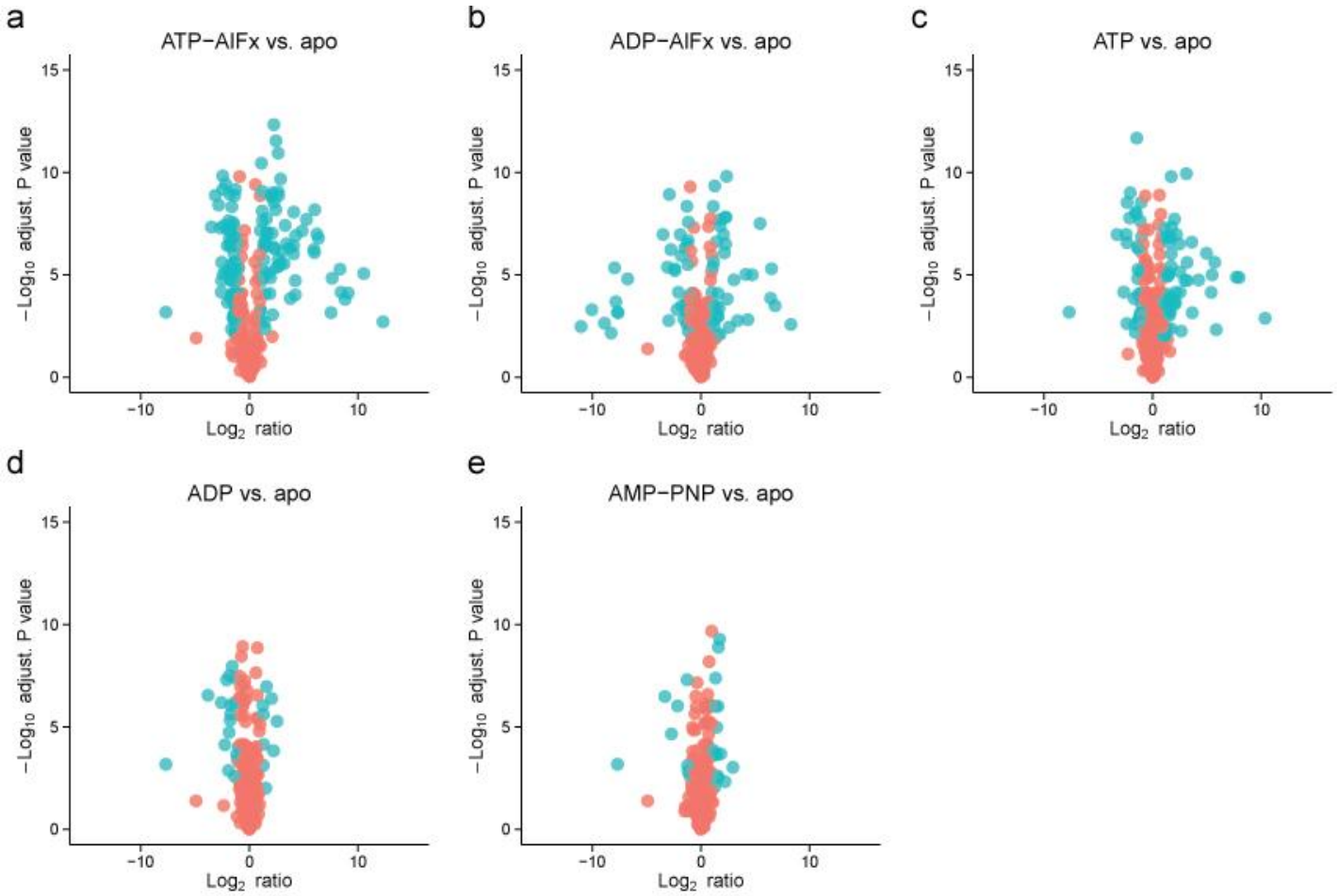

Supplementary Figure 12

Volcano plots of the TRiC transition states.

(**a–e**) Volcano plots of the different TRiC transition states compared against the apo state (LFQ-like workflow). Shown are the $\log_2$ ratios plotted against the adjusted negative $\log_{10}$ *P* values. Indicated by color is if the observed changes are significant (blue) or not (red) (adjusted *P* value < 0.01 and absolute $\log_2$ fold change >1).

Supplementary Table 1: Dilution factors for the dilution series experiment. Expected $\log_2$ fold changes are given in parentheses. For both workflows (LFQ-like and differential isotopic labeling) the same dilution factors were used.

Sample	Bovine serum albumin (BSA)	Bovine Transferrin	Chicken Conalbumin
1	1(0)	1(0)	1(0)
2	1(0)	2 (–1)	4 (–2)
3	1(0)	4 (–2)	16 (–4)
4	1(0)	8 (–3)	64 (–6)

Supplementary Results 1

The dilution series dataset was generated by cross-linking a panel of individual, purified proteins with known structures in different concentrations in two biochemical replicates. For the LFQ-like workflow the proteins were cross-linked with an equimolar mixture of light and heavy disuccinimidyl suberate (DSS-H_{12}/D_{12}, where H_{12} corresponds to the light version of the cross-linker and D_{12} to the heavy (deuterated) version of the cross-linker). For the differential isotopic labeling workflow, the proteins were cross-linked either with DSS-H_{12} or DSS-D_{12}.

After the cross-linking reaction the proteins were then mixed and diluted according to the quantities outlined in **Supplementary Table 1**. The proteins were then digested to peptides and fractionated by size exclusion chromatography[24] and analyzed by LC-MS/MS. The dataset was comprised of 48 LC-MS/MS runs for the LFQ-like workflow and 96 LC-MS/MS runs for the differential isotopic labeling workflow (see **Online methods** for details). Identification and statistical validation of cross-linked peptides from the dataset was carried out with the previously described xQuest and xProphet software pipeline[3] and led to the identification of 179 unique intra-protein cross-links, corresponding to 148 unique restraints (uxIDs) (**Supplementary Table 2**). The cross-linked peptides identified by the two workflows showed an overlap of 67% **(Supplementary Fig. 2)** and the cross-links were validated against high resolution X-ray structures showing good agreement with the selected FDR cutoff of 5% (**Supplementary Fig. 3**).

We next quantified the identified cross-linked peptides in the gold standard datasets and related the obtained quantitative values to the values expected from the dilution ratios used to generate the samples. To compare the samples we applied a simple normalization strategy for the LFQ-like workflow that is based on mean values of a set of reference or standard peptides (in our case, BSA peptides, since BSA was present at the same amount in all experiments). The retention time was controlled by a simple retention time normalization procedure based on linear regression using a set of common peptides between MS experiments. To restrict the quantification results to those that are trustworthy, *xTract-analyzer* applies a post extraction validation mechanism, i.e. it only considers identifications as valid if they have been consistently extracted in all replicates of an experimental condition (i.e. a certain state) or in none of the replicates of an experimental condition. To deal with peptides that have not been detected in one condition of an experiment, the fold change is estimated based on the detection limit of the mass spectrometer (**Online methods**).

The quantitative results for the 148 targeted uxIDs are shown in **Supplementary Fig. 4** (**Supplementary Table 3**). Further, the results obtained from the two quantification strategies are plotted against each other. Both workflows showed very good agreement among each other and to the expected values, as indicated by the horizontal lines for the uxIDs of the individual proteins. Comparable results were obtained when only the light cross-linker was used for quantification by the LFQ-like workflow (**Supplementary Fig. 4**). The relative numbers of *bona fide* quantifiable uxIDs, which are reduced compared to the number of identified uxIDs due to the post validation mechanism, varied from 75%–87% for the LFQ-like workflow and 82%– 89% for the differential isotopic label workflow. Furthermore, the results showed that the variance for the individual cross-link uxIDs was lower (in six out of nine comparisons) for the differential isotopic label workflow due to the fact that quantification is performed within a single MS experiment.

In summary, our results show that both quantification strategies generate comparable and accurate quantification results, even for low intensity cross-linked peptides. The differential isotopic label workflow was slightly more accurate, however it required a higher number of measurements (96 vs. 48 LC-MS/MS runs).

Supplementary Results 2

Enzyme activity during the cross-linking reaction

We monitored the activity of the enzyme during the cross-linking reaction using a luminescence assay (**Supplementary Fig. 5**). It showed a decrease in luminescence after the addition of the cross-linker, indicating that the enzyme was stalled by the cross-linking reaction, presumably due to its inability of adopting the domain rearranged active conformation.

Luciferase cross-linking data

Using the LFQ-like workflow the xQuest and xProphet pipeline identified 76 unique cross-links corresponding to 53 uxIDs. 60 unique cross-linked peptides (46 uxIDs) were identified for the apo experiment and 55 (37 uxIDs) for the activated conformational state at an FDR of 5% (**Supplementary Table 4**). Comparing the identifications we found that 39 unique cross-links (30 uxIDs) were identified in both experiments. Applying the quantitative workflow, xTract successfully quantified 45 uxIDs across both states. We found that 21 uxIDs showed a significant change (adjusted *P* value < 0.01 and absolute $\log_2$ fold change > 1) when comparing the activated to the apo state. The fold changes ranged from a 6.2-fold decrease to a 3.5-fold increase between the states (**Supplementary Fig. 6b)**. For the differential isotopic label workflow, we performed a forward and reverse labeling scheme (**Fig. 1, Step 3**) and a “Master-Mix” experiment to identify cross-links that were not detectable in one of the states and to serve as a control experiment. In this setup the forward experiment refers to labeling the apo state with the light cross-linker and the activated state with the heavy cross-linker. Reverse label refers to switching the labels for the states and serves as a control and replicate experiment. The Master-Mix experiment was a combination of the forward and reverse label experiments, which sums the intensities as if a 1:1 mixture of light and heavy cross-linker would have been used (**Supplementary Fig. 7a-c**). We chose this strategy because the presence of light and heavy labeled molecules facilitates the identification by xQuest.

For the differential isotopic label based workflow, including the forward, the reverse and the Master-Mix experiment we identified 82 unique cross-linked peptides (62 uxIDs) at an FDR of 5% (**Supplementary Table 5**). Comparing the workflows based on identifications showed that in total 95 unique cross-linked peptides (69 uxIDs) were

identified. The overlap between the different workflows was 66% (63 unique cross-links, 46 uxIDs).

We then compared the cross-links and their quantitative patterns obtained from the two quantification methods (**Supplementary Fig. 6a,b**). This analysis showed a high correlation of the datasets (R^2 = 0.899, **Fig. 4b**). The individual datasets obtained from the different workflows were then combined to maximize the yield of quantifiable cross-links. This allowed the quantification of 59 out of 69 uxIDs and 21 uxIDs showed a significant fold change (adjusted *P* value < 0.01 and absolute $\log_2$ fold change > 1, **Fig. 2c, Supplementary Table 6**), ranging from an 8.1-fold decrease to a 3.5-fold increase. Together these results show that both workflows are able to obtain consistent quantification results and supported the quantification of >85% of the observed unique restraints.

Luciferase dimer assembly

First, a manual solution was found (**Supplementary Fig. 8b**) that satisfied the majority of cross-links as either intra- or inter-molecular. As an independent control we performed an exhaustive low-resolution but unbiased docking analysis using ROSETTA[31]. The ensemble of dimeric structures was scored using the total energy score and the number of satisfied cross-links as selection criteria. The model that satisfied the highest number of restraints showed a convergence towards a low scoring model by score and was similar to that found manually (**Supplementary Fig. 8a,c**) amongst 248,424 randomly docked dimer structures. Finally, the manually identified dimeric state conformation was used and the dimer interface was refined using a high-resolution full-atom protocol using the ROSETTA software suite (**Fig. 2e,f**) and the best solution satisfied 27 of 28 uxIDs, which could be mapped onto the structure, a value that is also consistent with the selected FDR cutoff of 5%.

To validate conformational changes, we next generated molecular models of the luciferase dimer for the secondary conformations based on the refined apo dimer (**Supplementary Fig. 8d,e**).

Supplementary note 1

TRiC experiments

All experiments were carried out using two biochemical and two (or four) technical replicates. For quantification, we used the LFQ-like workflow for all states due to the larger number of samples and additionally used the differential isotopic label workflow as an independent control for comparing the ATP-AlFx and the apo state (**Supplementary Figure 11a-c**).

TRiC structural data

Due to the hetero-oligomeric nature of the complex, and the high structural similarity of the subunits it has been challenging to acquire and interpret structural information. Recently, a 3.8 Å ATP-AlFx state structure was determined by using CX-MS data and prior information, including low resolution X-ray diffraction data that was by itself not sufficient to solve the structure[11]. Additionally, a 5.5 Å apo state conformation is availaible[40, 50, 51]. Additionally, low resolution cryo-EM reconstructions for intermediate nucleotide conformations exist in the presence of ADP, ADP-AlFx and the non-hydrolyzable ATP analog AMP-PNP that fall between the symmetrically closed and the apo conformations[40].

Supplementary Results 3

TRiC quantitative data

When comparing the restraints of the different TRiC transition states against the apo state of TRiC, $\log_2$-fold changes ranging from –11 to +12 were detected. The largest number of significant (adjusted *P* value <0.01 and absolute $\log_2$ fold change >1) changes (145 uxIDs) were observed for the most divergent ATP-AlFx (closed) state and fewest significant changes were observed for the most similar states ADP (27 uxIDs) and AMP-PNP (25 uxIDs).

TRiC correlation analysis

The highest correlations were observed between apo, AMP-PNP and ADP (all Pearson correlation coefficients (PCCs) > 0.94) and ATP and AlFx (PCC > 0.90), while the lowest correlation was observed between apo and ATP-AlFx (PCC 0.48), corresponding to the two most divergent states (open and closed).

Supplementary Table 9: Replacement scheme for amino acids used for the decoy generation.

AA a	AA b
K	Y
E	F
H	M
R	W
Q	D
I	N
C	L
V	T
S	P
G	A

Supplementary References

50. Kalisman, N., Adams, C.M. & Levitt, M. Subunit order of eukaryotic TRiC/CCT chaperonin by cross-linking, mass spectrometry, and combinatorial homology modeling. *Proc. Natl. Acad. Sci. U S A* **109**, 2884-2889 (2012).
51. Munoz, I.G. *et al.* Crystal structure of the open conformation of the mammalian chaperonin CCT in complex with tubulin. *Nat. Struct. Mol. Biol.* **18**, 14-19 (2011).